--Supporting Information--

For

Valorization of waste polypropylene as a robust catalyst for rapid degradation of antibiotics in complex water matrices

Guohang Zhou[a,b], Zhenyan Liu[c], Hui Wang[c,*], Duqiang Zhang[a,b], Wenhao Li[a,b], Zhiguo Qu[c], Xin Wang[a,b,*]

[a] *Key Laboratory of Advanced Technologies of Materials (Ministry of Education), School of Material Science and Engineering, Southwest Jiaotong University, Chengdu 610031, China*

[b] *Research Institute of Frontier Science, Southwest Jiaotong University, Chengdu 610031, China*

[c] *MOE Key Laboratory of Thermo-Fluid Science and Engineering, Xi'an Jiaotong University, Xi'an 710049, China*

Corresponding authors:

Xin Wang, E-mail: xin.wang@swjtu.edu.cn

Hui Wang, E-mail: wanghui198@xjtu.edu.cn

Text S1. Chemicals and Reagents

Polypropylene (iPP, melt index 3.5g/10min) were provided by Zhonglian Plastics Technology Co., Ltd, Changzhou, China. Iron sulfate pentahydrate ($Fe_2(SO_4)_3 \cdot 5H_2O$) was purchased from Sinopharm Chemical Reagent Co., LTD., Shanghai, China. Peroxymonosulfate (PMS), tetracycline (TC), methanol (MeOH), tertbutyl alcohol (TBA), p-benzoquinone (p-BQ), furfuryl alcohol (FFA), L-histidine (L-his), β-carotene, sodium chloride (NaCl), humic acid (HA), ammonium dihydrogen phosphate ($NH_4H_2PO_4$), benzoic acid (BA), methyl phenyl sulfoxide (PMSO), methyl phenyl sulfone ($PMSO_2$), sodium hydroxide (NaOH), tetracycline (TC), sodium sulphate (Na_2SO_4), sodium hydrogen carbonate ($NaHCO_3$), sodium nitrate ($NaNO_3$) ammonium chloride (NH_4Cl), zinc chloride ($ZnCl_2$) and Nessler reagent were provided from Aladdin Biochemical Technology Co., Ltd, Shanghai, China. Concentrated sulfuric acid (H_2SO_4, purity 70%) was purchased from Kelong Chemical Co., Ltd, Chengdu, China. The abovementioned drugs were of analytical grade.

Text S2. Characterizations

The chemical structure of PP and PP-SO_3Fe were characterized by FT-IR (SPECTRUM ONE-B, Elmer Platinum, USA) (KBr tabletting method, scanning range: 400-4000cm^{-1}). The surface morphology of samples was characterized by using SEM (Sigma 360, Carl Zeiss Industrielle Messtechnik Co., Ltd., Germany) (gold plating on the surface; Electric field beam energy: 10kV) And Transmission electron microscopy (TEM) was operated (JEM-F200, JEOL Ltd., Japan) (Accelerating voltage: 200 kV) with energy dispersive spectroscopy (EDS) (X-Max^N 80T IE250, Oxford Instruments, USA). Metallographic images were characterized by using Metallographic microscope (UMT103i, Chongqing UOP Optoelectronic Technology Co., Ltd., China). The crystalline property was evaluated using a powder-XRD diffractometer (XRD-6100, Shimadzu Co., Ltd., Japan) (scanning voltage: 40 kV, scanning current: 30 mA, scanning angle: 5~70°, scanning speed: 5° min^{-1}). X-ray photoelectron spectroscopy (XPS) measurement was performed (K-Alpha, Thermo Fisher Scientific Co., Ltd., USA) to analyze elemental composition (X-ray source: Mono Al Kα; Energy: 1486.6 eV; Voltage: 12 KV; Beam current: 6 mA.). The test specimens were prepared by the KBr-disk method. X-ray absorption fine structure (XAFS) spectroscopy was carried out the (Rapid-XAFS 1M, Anhui Ab-using sorption Spectroscopy Analysis Instrument Co., Ltd.) (Transmission mode: 25 kV and 40 mA).

Text S3. Analytic methods

To test the Fe content in samples of varying proportions, a microwave digestion method was employed to convert the samples into solution, followed by Inductively coupled plasma emission spectrometry (ICP-OES) (iCAP 7000, Thermo Fisher Scientific Co., Ltd., USA) analysis to determine the Fe ion concentration. Specifically, 5 mg of sample was taken, mixed with 8 mL concentrated nitric acid and 2 mL hydrogen peroxide, then subjected to microwave digestion at 180 °C for 30 min at a power setting of 1000 W. The resulting digest was concentrated by heating to a volume of 5 mL. One milliliter of this solution was transferred to a 50 mL volumetric flask for ICP-OES analysis.

In the degradation of PMS-AOP as an oxidant, the target pollutants were generally degraded by the radical pathways of ·OH, $SO_4^{\cdot-}$, and $O_2^{\cdot-}$ and the non-radical pathways of $^1O_2$. EPR techniques (EMXplus-6/1, Bruker Co., Germany) and quenching experiments were used to identify the active species in this study. Add 20 mg of PP-SO_3Fe catalyst and 1 mM PMS to 100 mL of ultrapure water, then stirred at 400 rpm at room temperature and sonicate for 1 min. Take 30 μL of sample, added 30 μL DMPO (dissolved in 100 mM ultrapure water), mix thoroughly, then aspirate a measured volume of the mixture into a capillary tube. Place the tube into the EPR resonance chamber for testing ·OH, $SO_4^{\cdot-}$, and $O_2^{\cdot-}$ (The test point is set at 2 min). Additionally, the experiment includes radical testing with PMS alone. For singlet oxygen radical testing, take 30 μL of sample, add 50 μL of TEMP (100 mM), and follow the same testing conditions as above. Quenching experiments: A 20 mg of PP-SO_3Fe catalyst is added to 100 mL of a TC solution (50 mg/L). Subsequently, 1 M MeOH, 1M TBA, 50 mM p-BQ and 50 mM FFA was added separately, the mixture was stirred at 400 rpm for 5 min at room temperature. Finally, 1 mM PMS was added and started timing. 1 mL of aliquots were sampled at specific time intervals and quenched with 0.1 mL of 0.5 M $Na_2S_2O_3$ solution. The samples were filtered through 0.45 μm PTFE syringe filters and then determined for TC with HPLC.

TC concentration was quantified using high performance liquid chromatograph (HPLC) (LC-16, Shimadzu Co., Ltd., Japan) equipped with an ultraviolet detector (SPD-16). Separation was performed using a ShimNex CS C18 column (5 μm, 4.6 × 250 mm) maintained at 30 °C, with detection at 270 nm. The total collection time was 12 min, and the sample volume was 10 μL. The mobile phase consisted of an organic phase and a water phase (1:4, v/v) with a flow rate of 1ml/min. The mobile phase comprised an organic phase (methanol: acetonitrile, 1:3 v/v) and 0.01 M oxalic acid in the aqueous phase. The TC removal efficiency (η, %) was calculated using Eq. 1. Since the

degradation kinetics followed to a pseudo-first-order model, Eq. 2 was applied to fit the kinetic curve [1]:

$$\eta = \frac{C_0 - C_t}{C_0} \times 100\% \#(1)$$

$$\ln \frac{C_0}{C_t} = kt \#(2)$$

where C_0 (mg/L) is the initial TC concentration, C_t (mg/L) is the TC concentration at treatment time t, and k (min^{-1}) means rate constant.

NH_4^+ concentration was quantified using UV-vis spectrophotometer (UV-2600i, Shimadzu Co., Ltd., Japan) with detection at range of 200-600 nm. Take 5 mL of the solution, add 0.1 mL of Nessler reagent, mix thoroughly, and measure the absorbance after 10 min.

Total organic carbon (TOC-5000, Shanghai Metash Instruments Co., Ltd., China) was employed to determine the mineralization of TC in the catalyst/PMS system. All samples underwent rigorous acidification (to pH < 2) and inert gas purging prior to analysis to completely eliminate interference from dissolved inorganic carbon.

All Gas chromatography-mass spectroscopy technique (GC-MS) analyses were performed using an Agilent GC-6890N gas chromatograph coupled to a MS-5973N mass spectrometer (Agilent Technologies Co., Ltd., USA). Separation was achieved using an HP-5MS chromatographic column (30 m, 250 μm inner diameter, 0.25 μm film thickness) under the following conditions: helium carrier gas (1 mL/min) with auxiliary gas flow (40 mL/min); splitless injection at 250°C; transfer line temperature 280°C; oven temperature programmed from 60°C (hold for 2 min) to 300°C at 10°C/min (final hold for 5 min). A 2 μL injection volume was analyzed with a 0.2 s scan rate. Full-scan mass spectra (m/z 40-800) were acquired, and chromatographic peaks were identified through fragment interpretation complemented by NIST 11.0 database matching.

Text S4. Computational methods

The density functional theory calculations are performed using Gaussian 09 program [2]. The geometry optimization and frequency calculations were carried out at the B3LYP/6-311G** level. To account for the effects of the solvent, all calculations were performed using the solvation model density (SMD) continuum method [3] with water as the solvent. The highest occupied molecular orbital (HOMO), lowest unoccupied molecular orbital (LUMO) energies, and valence electron densities are compared to determine the reactivity of reactants. HOMO and LUMO orbital

composition analysis are based on natural atomic orbital (NAO) method. The Multiwfn and VMD programs are used for electronic wavefunction analysis and graphic drawing [4-6].

Text S5. Quantification of $^1O_2$

In PMS-AOPS, the consumption rate of FFA can serve as a reference for calculating the steady-state concentration of $^1O_2$, which can be obtained using the following equation [7].

$$-\frac{d[FFA]}{dt} = k_{FFA,\cdot OH}[\cdot OH]_{ss}[FFA] + k_{FFA,{}^1O_2}\left[{}^1O_2\right][FFA] \#(3)$$

Integrating Eq. 3 acquires,

$$-ln\frac{[FFA]}{[FFA]_0} = \left(k_{FFA,\cdot OH}[\cdot OH]_{ss,over} + k_{FFA,{}^1O_2}\left[{}^1O_2\right]_{ss,over}\right)t = k_{obs,FFA}t \#(4)$$

he $[FFA]_0$ was the initial concentration of FFA, and it was 50 mM in this work. [FFA] was the time-dependent concentration of FFA. $k_{FFA,\cdot OH}$ and $k_{FFA,\,1O2}$ were the second-order rate constants of the reaction of FFA with ·OH and $^1O_2$, and they were 3.6×10^9 $M^{-1}\cdot s^{-1}$ and 1.2×10^8 $M^{-1}\cdot s^{-1}$ in some works [8], $[\cdot OH]_{ss,over}$ and $[^1O_2]_{ss,over}$ were the steady-state concentrations of ·OH and $^1O_2$. $k_{obs,\,FFA}$ can be acquired from the equation of $\ln([FFA]/[FFA]_0) = k_{obs,\,FFA}$. Because of the absence of ·OH and $SO_4^{\cdot-}$, the Eq. 4 can be simplified as follows.

$$-ln\frac{[FFA]}{[FFA]_0} = k_{FFA,{}^1O_2}\left[{}^1O_2\right]_{ss,over}t = k_{obs,FFA}t \#(5)$$

hen, the $[^1O_2]_{ss,over}$ can be obtained by the following equation,

$$\left[{}^1O_2\right]_{ss,over} = \frac{k_{obs,FFA}}{k_{FFA,{}^1O_2}} \#(6)$$

Text S6. Quantification of Fe^{IV}=O

Similar to $^1O_2$, the concentration of Fe^{IV}=O can be determined by measuring the consumption of PMSO and the production of $PMSO_2$. The corresponding equations are as follows [8].

$$-\frac{d[PMSO_2]}{dt} = k_{PMSO,Fe^{IV}=O}\left[Fe^{IV}=O\right]_{ss,over}[PMSO] \#(7)$$

$$\eta = \frac{[PMSO_2]}{[PMSO]_0 - [PMSO]} \#(8)$$

Then, the value of [PMSO] in Eq. 6 was returned to the Eq. 7 and acquire a new Eq. 9.

$$-\frac{d[PMSO_2]}{[PMSO]_0-\frac{1}{\eta}[PMSO_2]}=k_{PMSO,Fe^{IV}=O}[Fe^{IV}=O]_{ss,over}dt \#(9)$$

Integrating Eq. 9 acquires,

$$\eta\, ln\frac{[PMSO]_0}{[PMSO]_0-\frac{1}{\eta}[PMSO_2]}=k_{PMSO,Fe^{IV}=O}[Fe^{IV}=O]_{ss,over}dt=k_{obs}t \#(10)$$

hen, the $[Fe^{IV}=O]_{ss,over}$ can be got as following,

$$[Fe^{IV}=O]_{ss,over}=\frac{k_{obs}}{k_{PMSO,Fe^{IV}=O}} \#(11)$$

In the above equation, the [PMSO], $[PMSO_2]$, $[Fe^{IV}=O]_{ss,over}$ were the steady-state concentrations concentration of PMSO, $PMSO_2$, and $Fe^{IV}=O$; $[PMSO]_0$ was the initial concentration of PMSO which was 100 μM in this work; η was the yield of $PMSO_2$ which was also known as the selectivity of $PMSO_2$; the $k_{PMSO,\ FeIV=O}$ was the second-order rate constant of PMSO with $Fe^{IV}=O$ and it was $1.23\times10^5\ M^{-1}\cdot s^{-1}$; k_{obs} can be obtained by the liner fitting of Eq. 10.

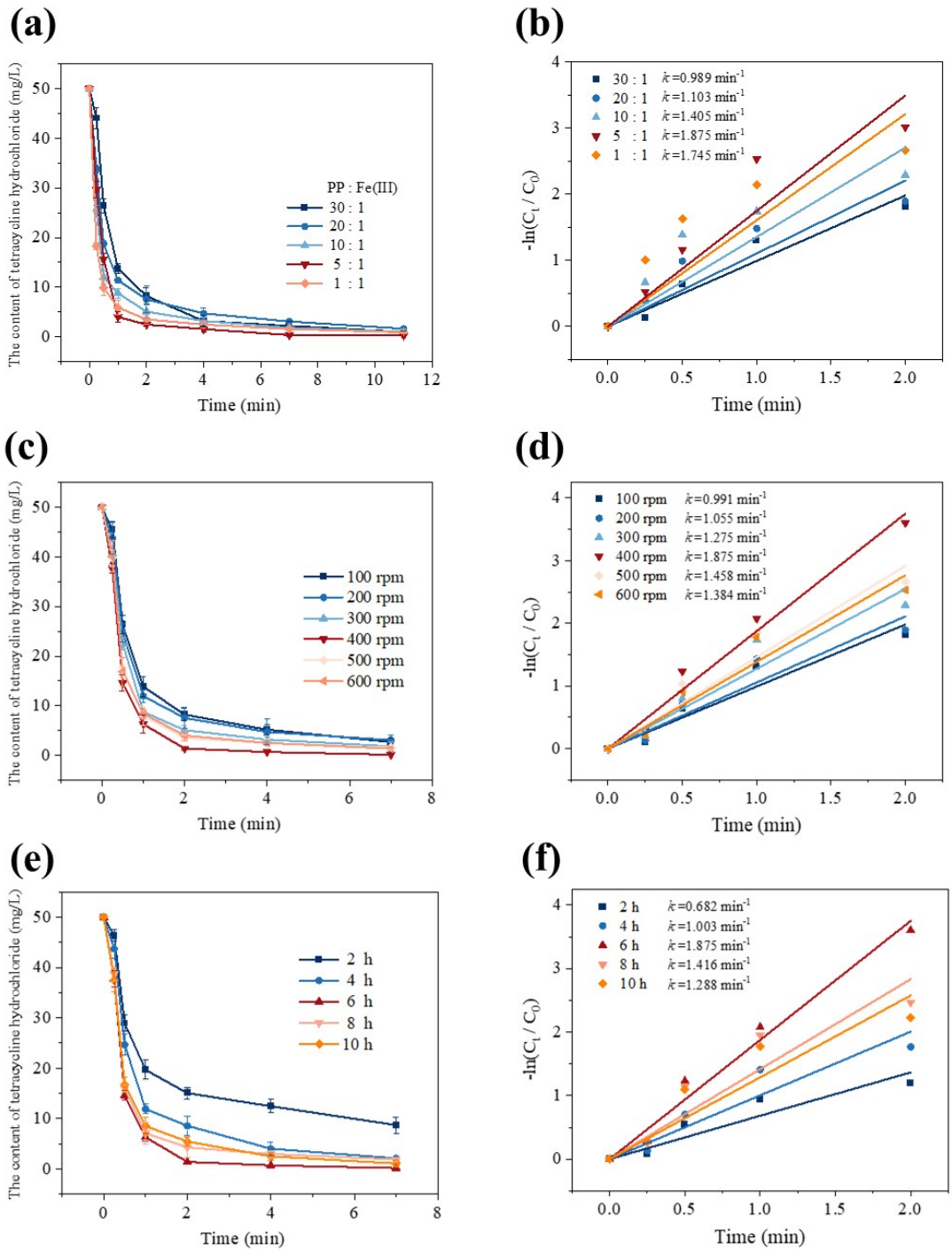

Fig. S1 Effect of (a, b) PP and Fe(III) mass ratio, (c, d) ball milling speed and (e, f) ball milling time on the TC degradation in Fe-functionalized PP/PMS system

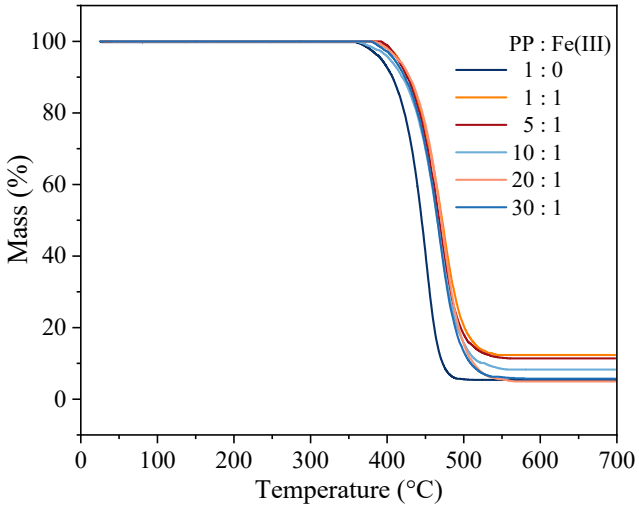

Fig. S2 Thermogravimetric analysis of samples with different mass ratios of PP and Fe(III).

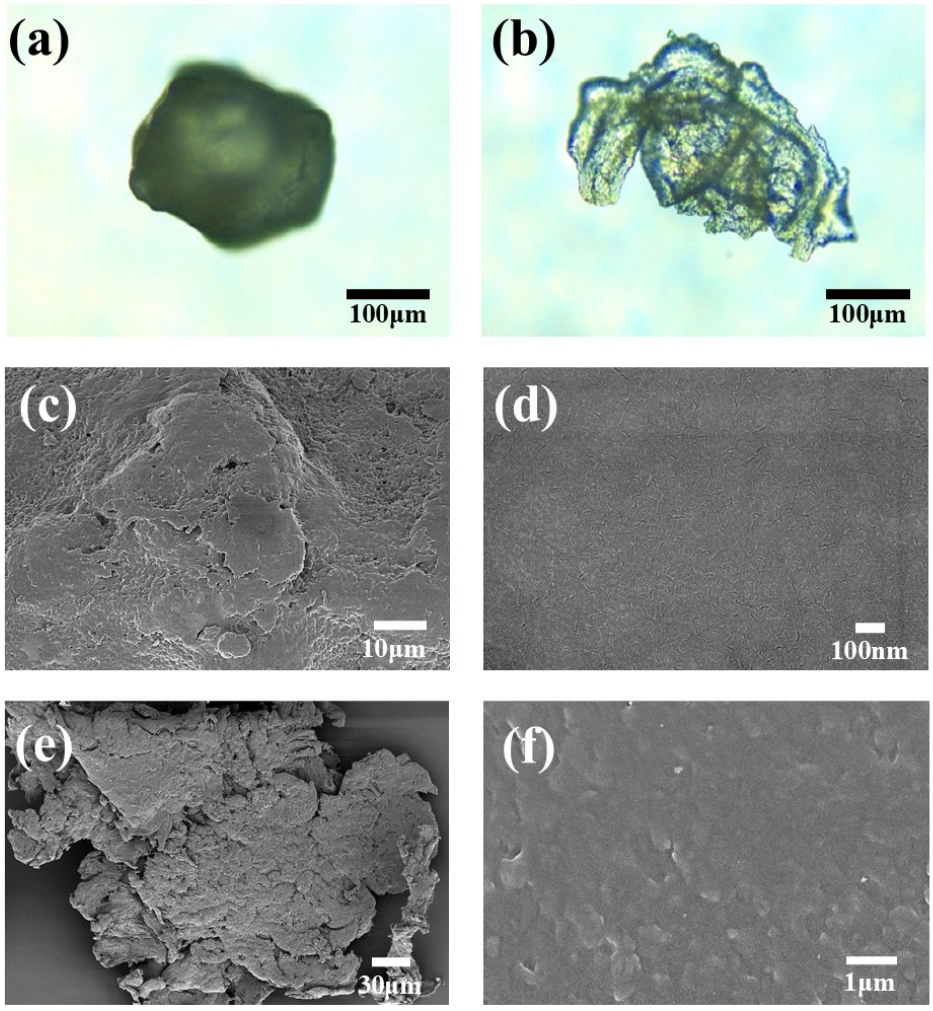

Fig. S3 (a, b) Metallographic microscope and (c, d) SEM images of PP and Fe-functionalized PP, and (e, f) the SEM images of PP treated with pure water.

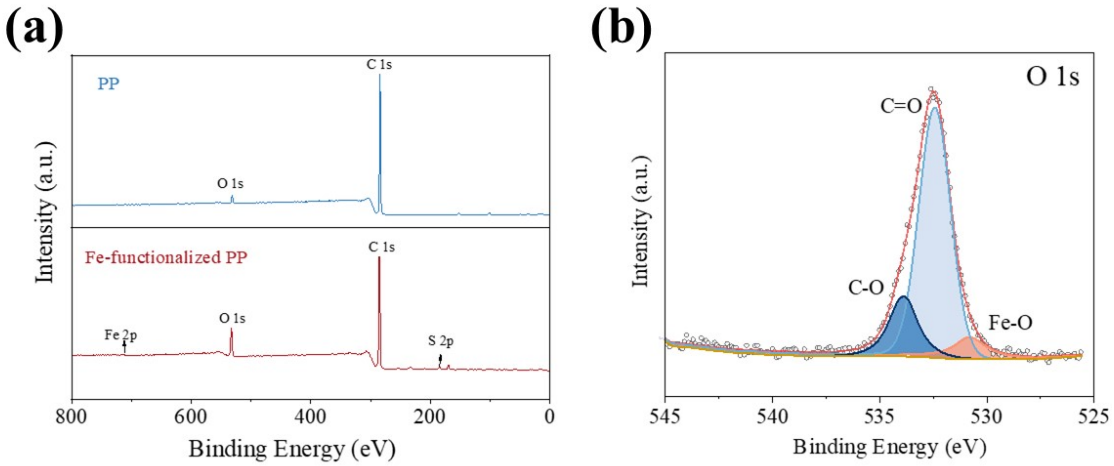

Fig. S4 (a) XPS survey of PP and Fe-functionalized PP and (b) high-resolution O 1s XPS spectrum of Fe-functionalized PP.

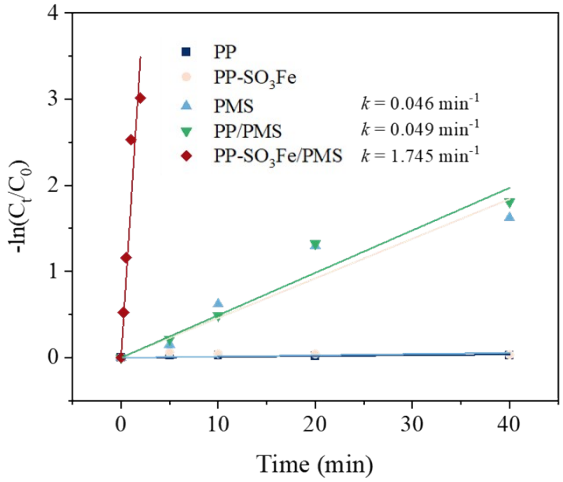

Fig. S5 Relative linear fit of the pseudo-first order kinetic model of TC degradation with various catalytic systems.

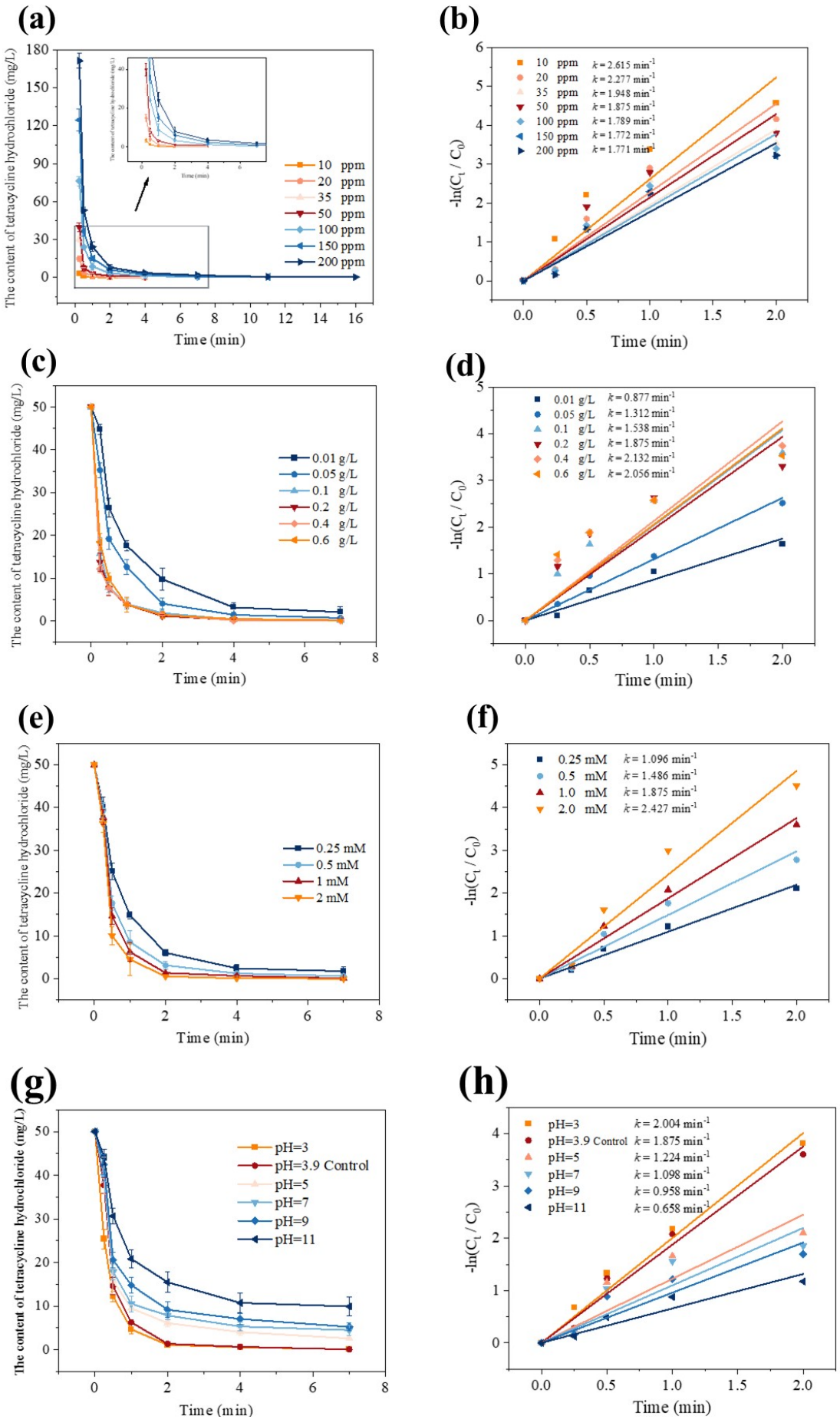
(a)
The content of tetracycline hydrochloride (mg/L)
Time (min)
10 ppm
20 ppm
35 ppm
50 ppm
100 ppm
150 ppm
200 ppm
(b)
-ln(C_t / C_0)
Time (min)
10 ppm k = 2.615 min-1
20 ppm k = 2.277 min-1
35 ppm k = 1.948 min-1
50 ppm k = 1.875 min-1
100 ppm k = 1.789 min-1
150 ppm k = 1.772 min-1
200 ppm k = 1.771 min-1
(c)
The content of tetracycline hydrochloride (mg/L)
Time (min)
0.01 g/L
0.05 g/L
0.1 g/L
0.2 g/L
0.4 g/L
0.6 g/L
(d)
-ln(C_t / C_0)
Time (min)
0.01 g/L k = 0.877 min-1
0.05 g/L k = 1.312 min-1
0.1 g/L k = 1.538 min-1
0.2 g/L k = 1.875 min-1
0.4 g/L k = 2.132 min-1
0.6 g/L k = 2.056 min-1
(e)
The content of tetracycline hydrochloride (mg/L)
Time (min)
0.25 mM
0.5 mM
1 mM
2 mM
(f)
-ln(C_t / C_0)
Time (min)
0.25 mM k = 1.096 min-1
0.5 mM k = 1.486 min-1
1.0 mM k = 1.875 min-1
2.0 mM k = 2.427 min-1
(g)
The content of tetracycline hydrochloride (mg/L)
Time (min)
pH=3
pH=3.9 Control
pH=5
pH=7
pH=9
pH=11
(h)
-ln(C_t / C_0)
Time (min)
pH=3 k = 2.004 min-1
pH=3.9 Control k = 1.875 min-1
pH=5 k = 1.224 min-1
pH=7 k = 1.098 min-1
pH=9 k = 0.958 min-1
pH=11 k = 0.658 min-1

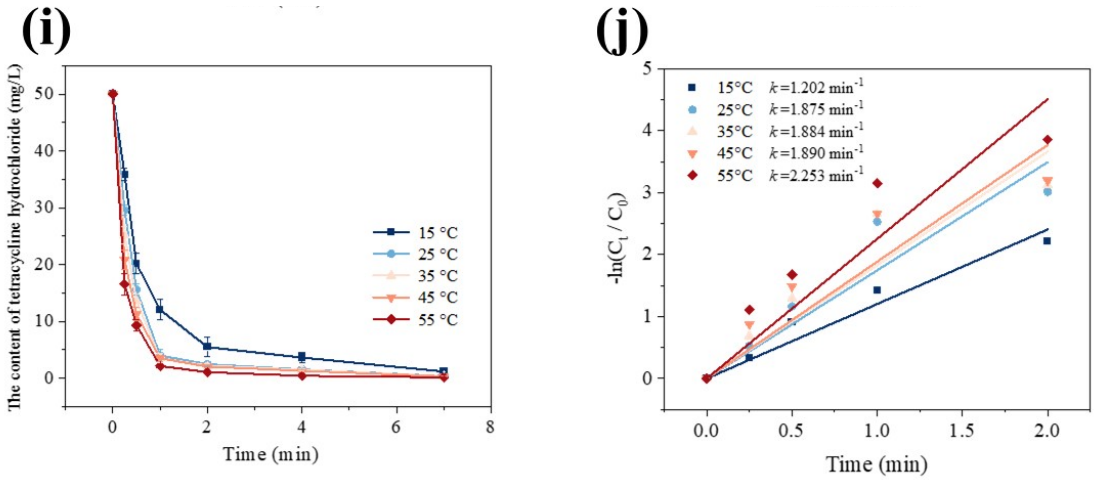

Fig. S6 Effects of (a, b) TC concentration, (c, d) PP-SO_3Fe dosage, (e, f) PMS concentration, (g, h) pH and (i, j) temperature on the degradation performance of TC with PP-SO_3Fe/PMS system.

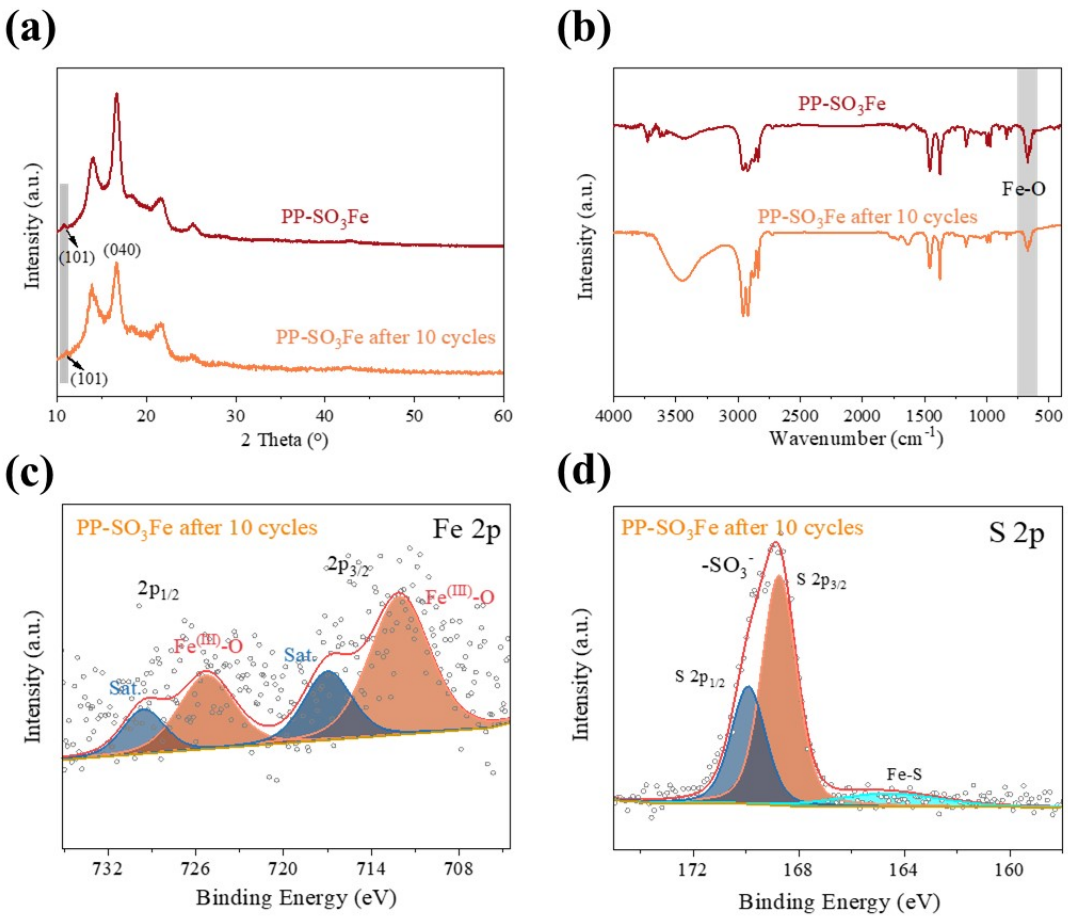

Fig. S7 (a) XRD patterns and (b) FTIR spectra of PP-SO_3Fe and PP-SO_3Fe after 10 cycles. The High-resolution (c) Fe 2p and (d) S 2p XPS spectra of PP-SO_3Fe after 10 cycles.

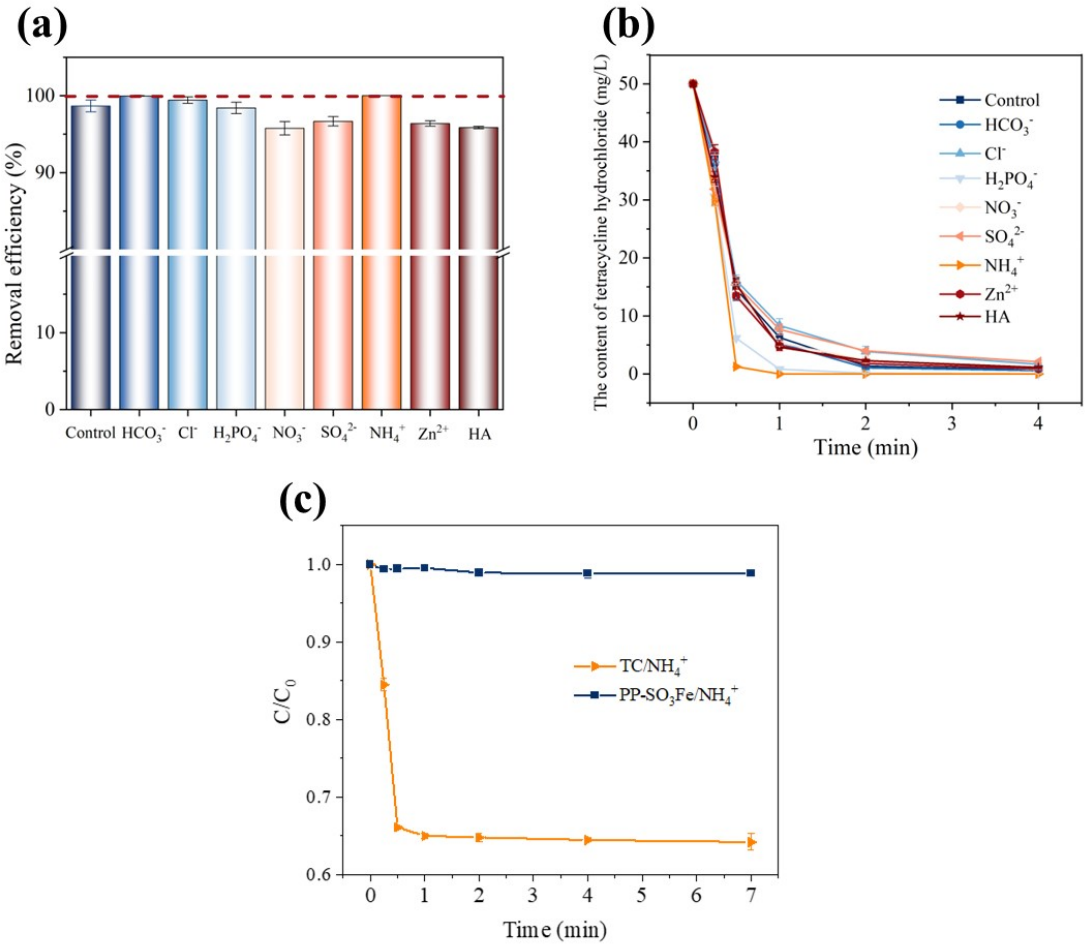

Fig. S8 The influences of coexistences in water for TC degradation with PP-SO_3Fe/PMS system (a) degradation curve, (b) removal efficiency comparison. (c) Adsorption isotherms of PP-SO_3Fe and TC for NH_4^+.

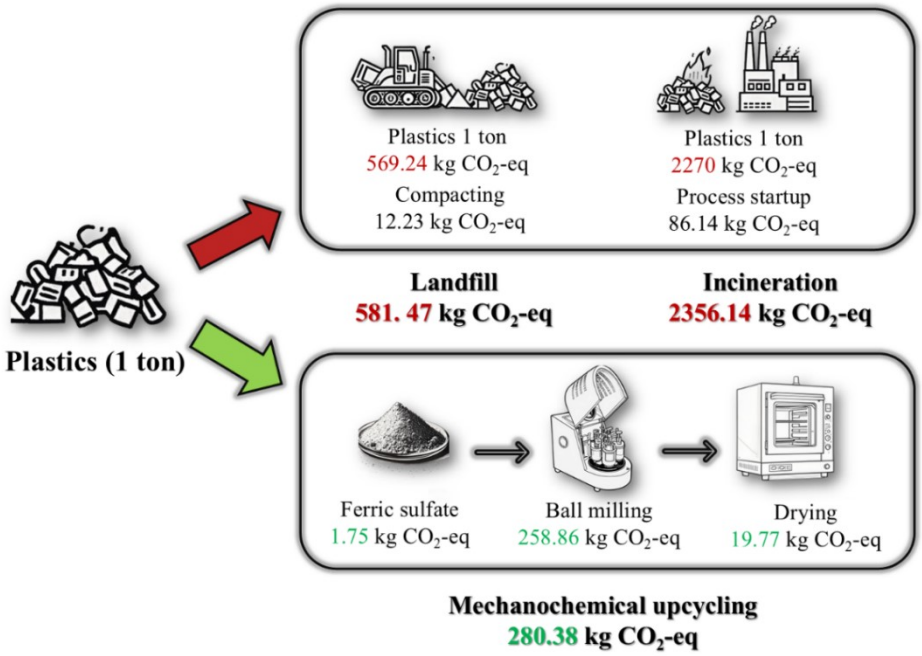

Fig. S9 Comparison of carbon emissions between landfill and incineration of waste plastics and

preparation of PP-SO_3Fe from waste plastics.

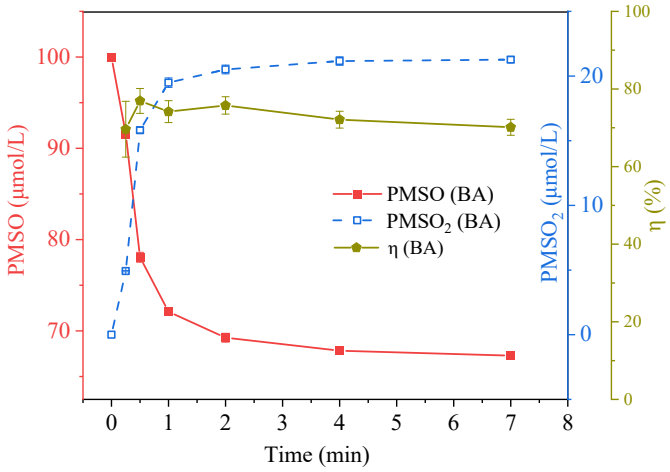

Fig. S10 PMSO consumption and $PMSO_2$ formation with BA, η ($PMSO_2$) values.

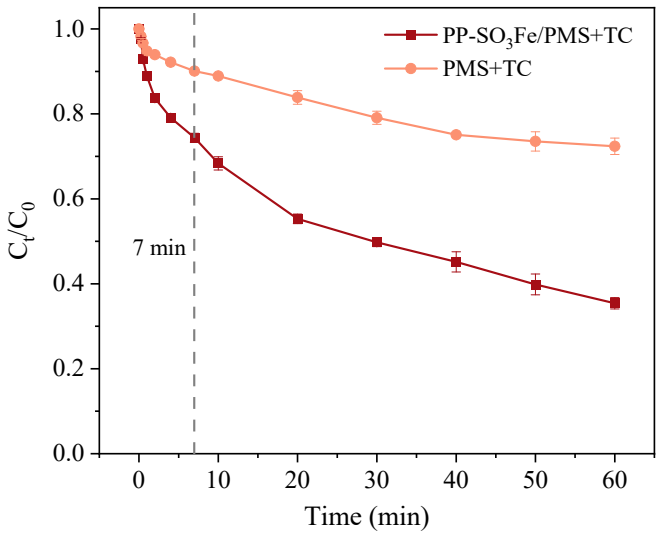

Fig. S11 TOC removal curves under different conditions.

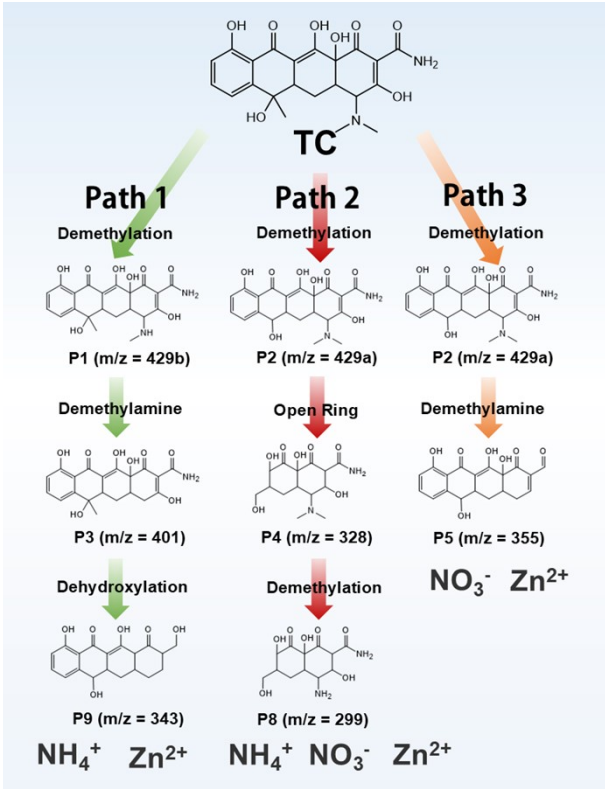

Fig. S12 Proposed pathways for TC degradation with ion-coexistence (NH_4^+, NO_3^- and Zn^{2+}) PP-SO_3Fe/PMS system.

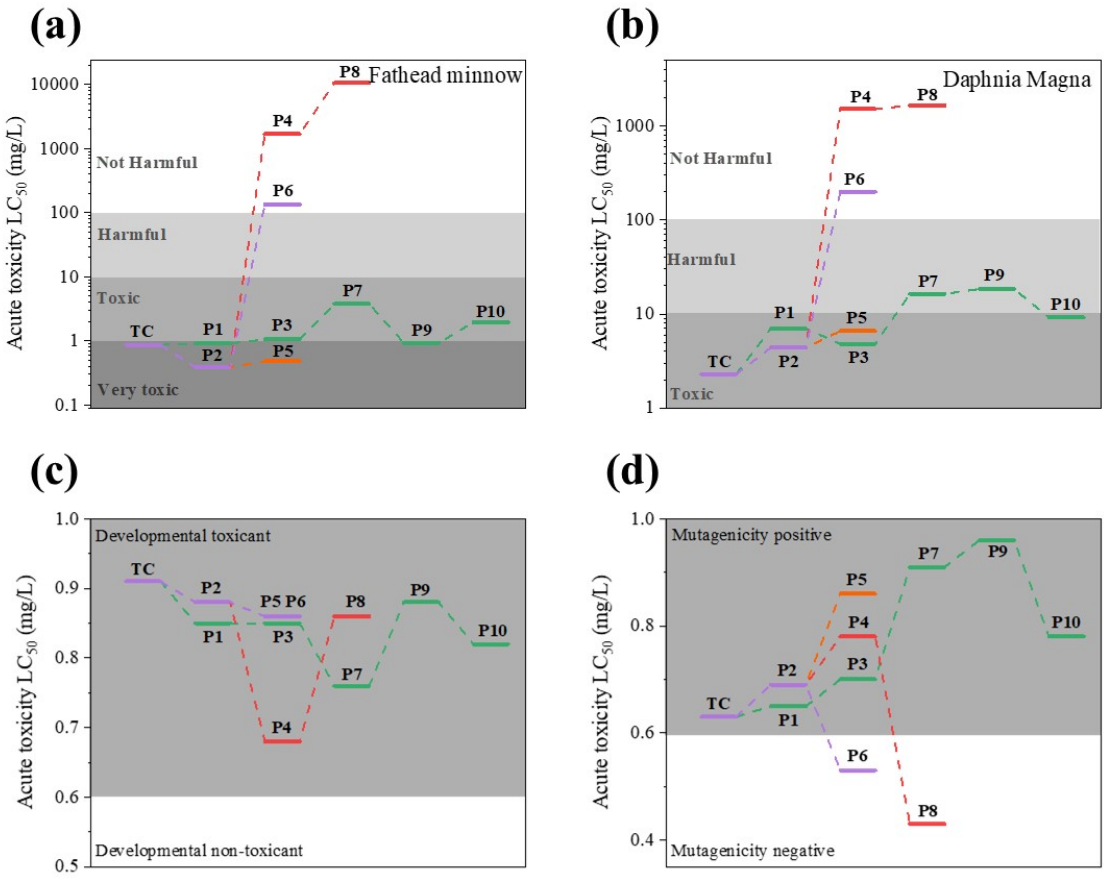

Fig. S13 Toxicity of (a) fathead minnow, (b) daphnia magna, (c) developmental toxicity, and (d) mutagenicity of TC and its degradation products by PP-SO_3Fe/PMS.

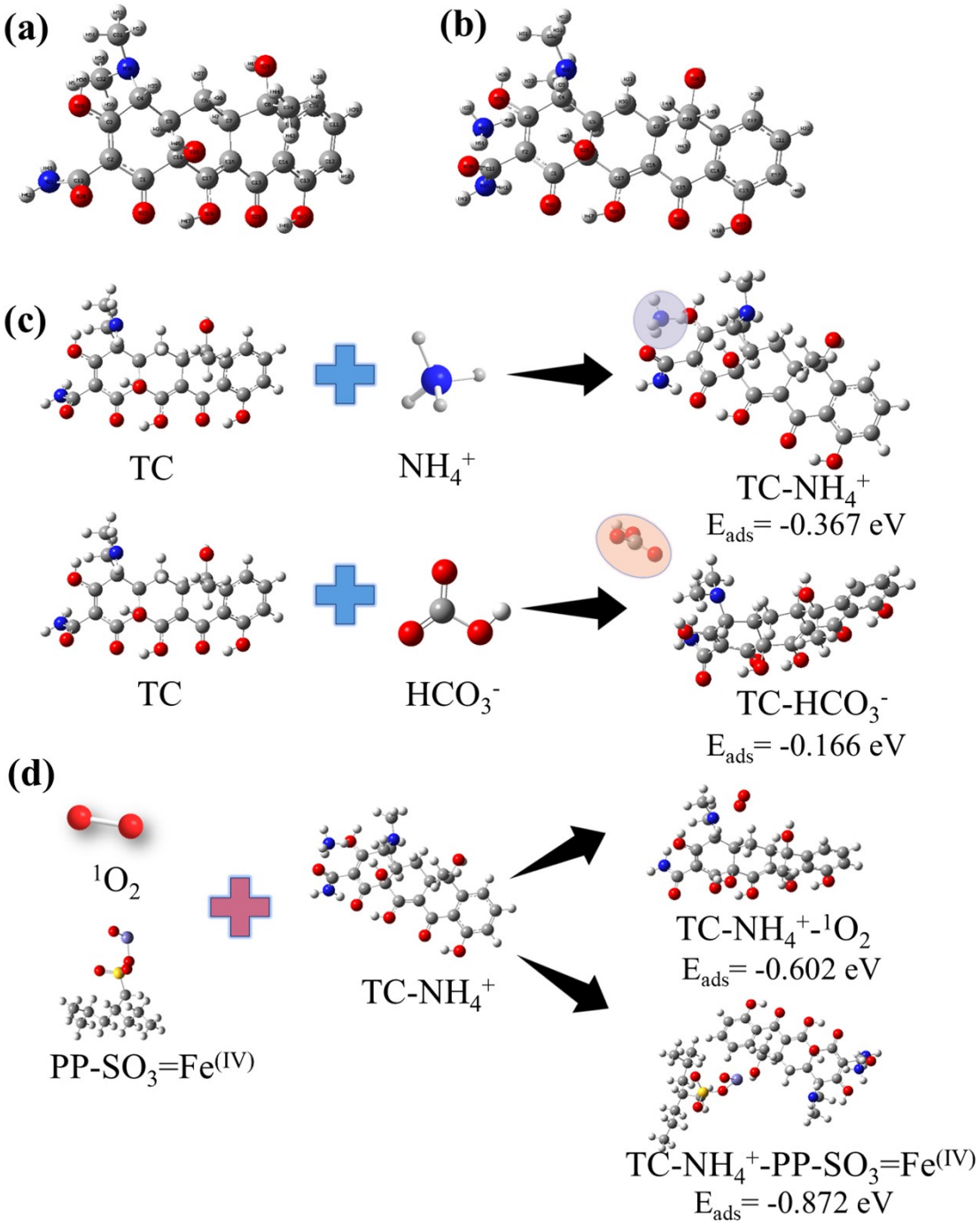

Fig. S14 The optimized structures of (a) TC and (b) TC-NH_4^+. (c) The adsorption binding energy between TC and NH_4^+ or HCO_3^-. (d) The adsorption binding energy with TC-NH_4^+ between $^1O_2$ and PP-SO_3=$Fe^{(IV)}$.

Table. S1 TGA and ICP-OES tests of samples with different mass ratios of PP and Fe(III)

The mass ratio of PP and Fe(III)	Weight loss ratio (%)	Fe loading (mg/g)
1:0	95.1	0
30 : 1	94.4	0.228
20 : 1	94.3	0.261
10 : 1	91.7	1.106
5 : 1	88.6	2.115
1 : 1	87.6	2.437

Table. S2 The EXAFS fitting parameters at the Fe K-edge for various samples (S_0^2=0.8)

Sample	Shell	R (Å) [a]	CN [b]	σ^2(Å^2) [c]	ΔE_0 (eV) [d]	R-factor [e]
PP-SO_3Fe	Fe-O	2.01±0.03	5.7±1.5	0.006±0.005	-2.7±3.2	0.017
PP-SO_3Fe/PMS	Fe-O	1.97±0.01	5.9±0.8	0.009±0.002	-4.9±1.7	0.010

Note: [a]. R: Bond length; [b]. CN: coordination number; [c]. σ^2: Debye-Waller factor; [d]. ΔE_0: edge-energy shift; [e]. R factor: goodness of fitting.

Table. S3. Ion concentrations in different water types.

Sample	NO_3^-	Cl^-	SO_4^{2-}	NH_4^+	pH
Industrial wastewater	41.5	475.9	520.2	0.6	5.4
Lake water	4.6	9.4	60.3	0.2	7.1
Tap water	33.5	4.7	21.4	0.1	7.7

Table. S4 Performance comparison of Fe-containing catalysts for PMS activation toward TC degradation.

Sample	Time (min)	Catalst (g/L)	PMS (mM)	TC (mg/L)	Removal efficient	Ref.
Fe-Cu@SNC	11	0.1	0.1 mM	10	82.0%	9
Fe-N/C	20	0.1	0.5 mM	20	89.4%	10
Fe@SUBC	90	0.6	0.1 g/L	10	90.0%	11
FeOOH@EPE	14	0.3	1 mM	20	96.7%	12
$CoFe_2S_4$/CNTs	30	0.02	0.01 g/L	1	98.7%	13
MoS_2/Fe(II)	20	0.05	1 mM	30	93.2%	14
FMDS-3	60	0.2	3 mM	40	90.7%	15
Fe-O-BC	60	2	5 mM	88	99.1%	16
PP-SO_3Fe	7	0.2	1 mM	50	98.7%	This work

Table S5 Inventory data related to plastic landfill, incineration and preparation of PP-SO_3Fe

Input parameters	Unit	Data	Global warming (kg CO_2-eq)	Sources
(a) Landfill				
Waste plastics	ton	1	569.24	[2]
Electricity- compacting the waste	kWh	11.1	12.23	Electricity, low voltage {CN}| market group for | Cut-off, U
(b) Incineration				
Waste plastics	ton	1	2270	[2]
Electricity- Process startup	kWh	78.2	86.14	Electricity, low voltage {CN}| market group for | Cut-off, U
(c) Preparation of PP-SO_3Fe				
PP	ton	1		
Iron sulfate	kg	6	1.75	Iron sulfate {RoW}| market for iron sulfate | Cut-off, U
Electricity- Ball milling	kWh	235	258.86	Electricity, low voltage {CN}| market group for | Cut-off, U
Electricity- Drying	kWh	18	19.77	

Table. S6 The atomic HOMO-LUMO contributions for TC and TC-NH_4.

TC			TC-NH_4		
Center	HOMO Composition	LUMO Composition	Center	HOMO Composition	LUMO Composition
1 (C)	0.19%	8.05%	1 (C)	0.18%	11.92%
2 (C)	1.76%	0.16%	2 (C)	1.66%	0.29%
3 (C)	3.40%	6.69%	3 (C)	3.31%	10.34%
4 (C)	0.91%	0.13%	4 (C)	0.87%	0.15%
5 (C)	2.06%	0.16%	5 (C)	2.04%	0.19%
6 (C)	0.56%	0.05%	6 (C)	0.56%	0.05%
7 (C)	0.09%	0.30%	7 (C)	0.11%	0.27%
8 (C)	0.01%	0.05%	8 (C)	0.00%	0.05%
9 (C)	0.03%	5.52%	9 (C)	0.04%	4.49%
10 (C)	0.25%	0.05%	10 (C)	0.38%	0.04%
11 (C)	0.03%	7.69%	11 (C)	0.05%	6.25%
12 (C)	0.12%	0.88%	12 (C)	0.17%	0.68%
13 (C)	0.14%	5.00%	13 (C)	0.23%	4.13%
14 (C)	0.10%	1.19%	14 (C)	0.18%	0.89%
15 (C)	0.02%	18.90%	15 (C)	0.02%	15.79%
16 (C)	0.52%	1.25%	16 (C)	0.84%	1.28%

TC			$TC\text{-}NH_4$		
Center	HOMO Composition	LUMO Composition	Center	HOMO Composition	LUMO Composition
17 (C)	0.35%	13.80%	17 (C)	0.46%	11.67%
18 (C)	0.18%	1.57%	18 (C)	0.16%	1.72%
19 (C)	0.27%	0.02%	19 (C)	0.25%	0.01%
20 (O)	0.30%	0.02%	20 (O)	0.04%	0.01%
21 (N)	0.14%	0.02%	21 (N)	0.09%	0.01%
22 (O)	0.06%	12.09%	22 (O)	0.09%	10.20%
23 (O)	0.53%	4.99%	23 (O)	0.48%	7.32%
24 (C)	0.01%	0.30%	24 (C)	0.01%	0.25%
25 (O)	0.06%	2.40%	25 (O)	0.08%	2.61%
26 (O)	0.22%	3.73%	26 (O)	0.35%	3.16%
27 (O)	0.20%	1.58%	27 (O)	0.33%	1.31%
28 (O)	0.00%	0.08%	28 (O)	0.01%	0.07%
29 (O)	0.43%	1.67%	29 (O)	0.41%	2.56%
30 (N)	66.83%	0.36%	30 (N)	66.34%	0.53%
31 (C)	2.22%	0.02%	31 (C)	2.23%	0.03%
32 (C)	2.30%	0.02%	32 (C)	2.32%	0.03%
33 (H)	0.01%	0.07%	33 (H)	0.01%	0.08%
34 (H)	0.14%	0.06%	34 (H)	0.20%	0.06%
35 (H)	0.01%	0.68%	35 (H)	0.01%	1.00%
36 (H)	0.13%	0.03%	36 (H)	0.15%	0.03%
37 (H)	0.05%	0.03%	37 (H)	0.05%	0.04%
38 (H)	0.00%	0.00%	38 (H)	0.00%	0.00%
39 (H)	0.00%	0.01%	39 (H)	0.00%	0.00%
40 (H)	0.00%	0.00%	40 (H)	0.00%	0.00%
41 (H)	0.02%	0.00%	41 (H)	0.01%	0.00%
42 (H)	0.05%	0.00%	42 (H)	0.05%	0.00%
43 (H)	0.00%	0.02%	43 (H)	0.00%	0.02%
44 (H)	0.00%	0.03%	44 (H)	0.00%	0.03%
45 (H)	0.00%	0.01%	45 (H)	0.00%	0.00%
46 (H)	0.00%	0.24%	46 (H)	0.00%	0.23%
47 (H)	0.01%	0.02%	47 (H)	0.01%	0.02%
48 (H)	0.00%	0.01%	48 (H)	0.00%	0.01%
49 (H)	0.00%	0.03%	49 (H)	0.00%	0.03%
50 (H)	0.03%	0.02%	50 (H)	0.02%	0.02%
51 (H)	5.81%	0.02%	51 (H)	5.78%	0.03%
52 (H)	1.86%	0.00%	52 (H)	1.83%	0.01%
53 (H)	0.28%	0.01%	53 (H)	0.28%	0.01%
54 (H)	1.40%	0.00%	54 (H)	1.40%	0.00%
55 (H)	5.56%	0.00%	55 (H)	5.54%	0.01%
56 (H)	0.40%	0.01%	56 (H)	0.39%	0.01%
			57 (N)	0.01%	0.01%

TC			$TC-NH_4$		
Center	HOMO Composition	LUMO Composition	Center	HOMO Composition	LUMO Composition
			58 (H)	0.00%	0.01%
			59 (H)	0.00%	0.02%
			60 (H)	0.00%	0.04%
			61 (H)	0.00%	0.00%

Reference

1. Y. Liu, C. Gao, L. Liu, Y. Li and X. Guo, Water Research, 2025, 286, 124177.
2. Y. Chen, Z. Cui, X. Cui, W. Liu, X. Wang, X. Li and S. Li, Resources, Conservation and Recycling, 2019, 146, 348-357.
3. M. Frisch, Inc, Wallingford CT, 2009, 201.
4. A. V. Marenich, C. J. Cramer and D. G. Truhlar, The Journal of Physical Chemistry B, 2009, 113, 6378-6396.
5. T. Lu and F. Chen, Journal of computational chemistry, 2012, 33, 580-592.
6. W. Humphrey, A. Dalke and K. Schulten, Journal of molecular graphics, 1996, 14, 33-38.
7. G. Wang, D. Huang, M. Cheng, L. Du, S. Chen, W. Zhou, R. Li, S. Li, H. Huang and W. Xu, Small, 2024, 20, 2401970.
8. Y. Lin, Y. Wang, Z. Weng, Y. Zhou, S. Liu, X. Ou, X. Xu, Y. Cai, J. Jiang and B. Han, Nature Communications, 2024, 15, 10032.
9. X. You, C. Wang, C. Wang, X. Xu, Y. Hu, N. Li, F. Hu, W. Liu and X. Peng, Journal of Colloid and Interface Science, 2025, 689, 137277.
10. Z. Yan, X. Zhao, C. Zhong, W. Gao, Y. Feng and J. Liu, Separation and Purification Technology, 2025, 354, 129489.
11. Y. Shan, B. Song, G. Ku, L. Wang, Z. Wang, C. Chen, N. A. Oladoja, J. Ali, E. M. Glebov and X. Zhuang, Journal of Environmental Chemical Engineering, 2026, 122541.
12. S. Liu, H. Guo, Z. Xu, Z. Li and X. Qi, Journal of Materials Science: Materials in Electronics, 2024, 35, 1747.
13. M. Wang, J. Wang, G. Wu, Q. Shen, W. Zhang, J. Guo, L. Huang, L. Feng, C. Yuan and F. Sun, Separation and Purification Technology, 2025, 363, 131972.
14. Z. Yan, F. He, J. Zhang, J. Fang, J. Wang and H. Zhou, Journal of Environmental Chemical Engineering, 2022, 10, 108860.
15. P. Chen, Z. Cheng, X. Zhang, C. Yan, J. Wei, F. Qiu and Y. Liu, Journal of Cleaner Production, 2024, 445, 141365.
16. Y. Tao, S. Sun, Y. Hu, S. Gong, S. Bao, H. Li, X. Zhang, Z. Yuan and X. Wu, Catalysts, 2024, 14, 556.